Solid State Sciences 13 (2011) 251–256

Contents lists available at ScienceDirect

Solid State Sciences

journal homepage: www.elsevier.com/locate/ssscie

X-ray analysis of ZnO nanoparticles by Williamson–Hall and size–strain plot methods

A. Khorsand Zak [a,b,*], W.H. Abd. Majid [a], M.E. Abrishami [b], Ramin Yousefi [c]

[a] Low Dimensional Material Research Center, Department of Physics, University of Malaya, Kuala Lumpur 50603, Malaysia
[b] Electroceramics Laboratory, Department of physics, Ferdowsi University of Mashhad, Iran
[c] Department of Physics, Islamic Azad University, Masjed-Soliman Branch, Masjed-Soliman, Iran

ARTICLE INFO

Article history:
Received 19 April 2010
Received in revised form
6 November 2010
Accepted 17 November 2010
Available online 24 November 2010

Keywords:
X-ray analysis
ZnO
Nanoparticle
Sol–gel synthesis

ABSTRACT

ZnO nanoparticles (ZnO-NPs) were prepared by a sol–gel combustion method from a zinc acetate precursor and acetic acid. The ZnO-NPs were synthesized at calcination temperatures of 650 °C and 750 °C for 1 h. The synthesized ZnO-NPs were characterized by X-ray diffraction analysis (XRD) and TEM. The XRD results revealed that the sample product was crystalline with a hexagonal wurtzite phase. High-magnification transmission electron microscopy (TEM) showed single-crystal ZnO-NPs with nearly spherical shapes. The crystalline development in the ZnO-NPs was investigated by X-ray peak broadening. The Williamson–Hall (W–H) analysis and size–strain plot method were used to study the individual contributions of crystallite sizes and lattice strain on the peak broadening of the ZnO-NPs. The physical parameters such as strain, stress and energy density values were calculated more precisely for all the reflection peaks of XRD corresponding to the wurtzite hexagonal phase of ZnO lying in the range of 20°–100° from the modified form of the W–H plot assuming a uniform deformation model (UDM), uniform stress deformation model (USDM), uniform deformation energy density model (UDEDM) and by the size–strain plot method (SSP). The results obtained showed that the mean particle size of the ZnO-NPs estimated from the TEM, W–H analysis and the SSP method were highly intercorrelated.

1. Introduction

Zinc oxide (ZnO) is known as an important semiconductor which has been studied extensively in the past few years due to its fundamental and technological importance. Its many attractive properties, such as wide bandgap (3.37 eV), large exciton binding energy and excellent chemical stability, suggest a great many possible practical applications such as in gas sensors, ceramics, field-emission devices and luminescent materials [1–3]. Particle size and crystal morphology play important roles in these applications, which have driven researchers to focus on the synthesis of nanocrystalline ZnO in recent years. Therefore, many methods, including sol–gel [4] and solo-chemical processes [5], precipitation [6], combustion synthesis [7], DC thermal plasma synthesis [8], spray pyrolysis [9], pyrolysis [10], hydrothermal synthesis [11,12] and others, have been developed to prepare ZnO nanopowders.

A perfect crystal would extend infinitely in all directions; therefore, no crystals are perfect due to their finite size. This deviation from perfect crystallinity leads to a broadening of the diffraction peaks. The two main properties extracted from peak width analysis are the crystallite size and lattice strain. Crystallite size is a measure of the size of coherently diffracting domains. The crystallite size of the particles is not generally the same as the particle size due to the formation of polycrystalline aggregates [13]. Lattice strain is a measure of the distribution of lattice constants arising from crystal imperfections, such as lattice dislocations. Other sources of strain include the grain boundary triple junction, contact or sinter stresses, stacking faults and coherency stresses [14]. Crystallite size and lattice strain affect the Bragg peak in different ways. Both these effects increase the peak width and intensity and shift the 2θ peak position accordingly. The effect of strain, both uniform and nonuniform, on the direction of X-ray reflection is illustrated in Fig. 1. A portion of an unstrained grain appears in panel (a) on the left, and the set of transverse reflecting planes shown has a uniform equilibrium spacing d. The diffraction line from these planes appears on the right. If a uniform tensile strain is applied to a grain at right angles to the reflecting planes, their spacing becomes larger than d and the corresponding diffraction line shifts to lower angles but does not otherwise change, as shown in panel (b). This line shift is the basis of the X-ray method for the measurement of macrostress. In (c) the grain is bent and the strain is nonuniform; on the top (tension) side

* Corresponding author. Low Dimensional Material Research Center, Solid state laboratory, Department of Physics, University of Malaya, Kuala Lumpur 50603, Malaysia. Tel.: +60 12 2850849; fax: +60 37 9674146.
E-mail address: alikhorsandzak@gmail.com (A. Khorsand Zak).

1293-2558/$ – see front matter © 2010 Elsevier Masson SAS. All rights reserved.
doi:10.1016/j.solidstatesciences.2010.11.024

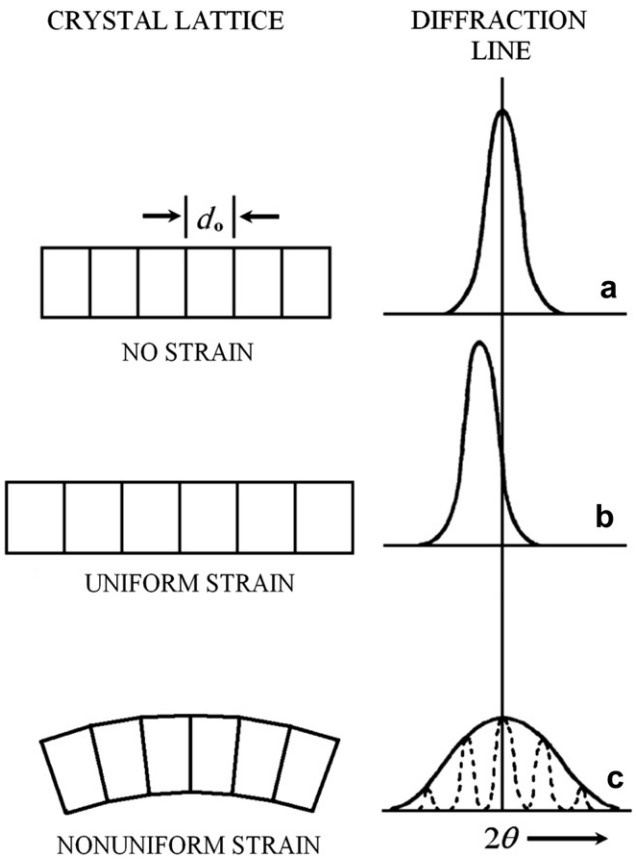

Fig. 1. A portion of an unstrained grain appears in (a), uniform tensile strain (b) and nonuniform strain (c). According to the figure the uniform strain affect the peak position and the nonuniform strain affect the peak broadening and intensity.

the plane spacing exceeds d, whereas on the bottom (compression) side it is less than d, and somewhere in between it equals d_o [15].

However, the peak width derived from crystallite size varies as $1/cos\theta$, whereas strain varies as $tan\theta$. This difference in behavior as a function of 2θ enables one to discriminate between the size and strain effects on peak broadening. The Bragg width contribution from crystallite size is inversely proportional to the crystallite size [16]. W–H analysis is a simplified integral breadth method where size-induced and strain-induced broadening are deconvoluted by considering the peak width as a function of 2θ [17]. Although X-ray profile analysis is an averaging method, apart from TEM imaging, it still holds a dominant position in grain-size determination.

In this study, a sol–gel combustion method was used to prepare ZnO-NPs. In addition, a comparative evaluation of the mean particle size of the ZnO-NPs obtained from direct TEM measurements and from powder XRD procedures is reported. The strain due to lattice deformation associated with the ZnO-NPs calcined at 650 °C and 700 °C was estimated by a modified form of W–H, namely uniform deformation model (UDM). The other modified models, such as uniform stress deformation model (USDM), uniform deformation energy-density model (UDEDM) and the size–strain plot method (SSP) provided information on the stress–strain relation and the strain ε as a function of energy density, (u).

2. Experimental

2.1. Sample synthesis and geometric characterization

To prepare 10 g of ZnO-NPs, 135 mL pure water was mixed with 65 mL isopropanol and the mixed solution was stirred for 5 min at 30 °C. Then the temperature was increased to 45 °C and zinc acetate was gradually added to the solution. After 30 min, 50 mL acetic acid was added to the clear solution and it was stirred again for 30 min at 40 °C. The prepared sol was refluxed for 4 h at 110 °C. The container of the solution was placed in the water bath and the temperature was kept at 80 °C for 16 h to prepare a viscous gel from the refluxed sol. Finally, a xerogel was obtained by treating the gel with nitric acid. The xerogel was then calcined for 2 h at 650 °C or 750 °C to obtain a white ZnO-NP powder. Phase evolutions of the ZnO-NPs were studied by X-ray diffractometry. The complete procedure can be found in the literature [24].

3. Results and discussion

3.1. XRD analysis

The XRD patterns of the prepared samples are shown in Fig. 2. All the detectable peaks could be indexed as the ZnO wurtzite structure found in the standard reference data (JCPDS: 36–1451). It was clearly seen that the reflection peaks became sharper with increasing calcination temperature, indicating the enhancement of crystallinity. The wurtzite lattice parameters such as the values of d, the distance between adjacent planes in the Miller indices (hkl) (calculated from the Bragg equation, $\lambda = 2d\,sin\theta$), lattice constants a, b, and c, interplanar angle (the angle φ between the planes ($h_1k_1l_1$), of spacing d_1 and the plane ($h_2k_2l_2$) of spacing d_2), and unit cell volumes are calculated from the *Lattice Geometry* equation as presented below [18]. The lattice parameters of the powders calcined at different temperatures are summarized in Table 1.

$$\frac{1}{d^2} = \frac{4}{3}\left(\frac{h^2 + hk + k^2}{a^2}\right) + \frac{l^2}{c^2} \tag{1}$$

$$V = \frac{\sqrt{3}a^2c}{2} = 0.866a^2c \tag{2}$$

$$\cos\varphi = \frac{h_1h_2 + k_1k_2 + \frac{1}{2}(h_1k_2 + h_2k_1) + \frac{3a^2}{4c^2}l_1l_2}{\sqrt{\left(h_1^2 + k_1^2 + h_1k_1 + \frac{3a^2}{4c^2}l_1^2\right)\left(h_2^2 + k_2^2 + h_2k_2 + \frac{3a^2}{4c^2}l_2^2\right)}} \tag{3}$$

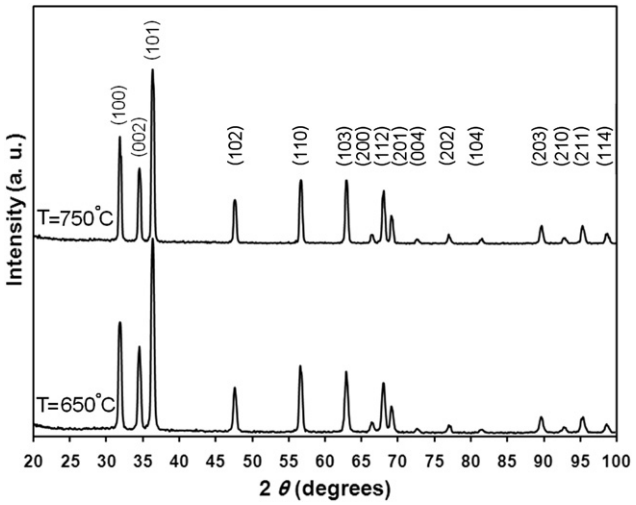

Fig. 2. The XRD pattern of ZnO-NPs calcinated at 650 °C and 750 °C. The XRD pattern shows that the sample product is crystalline with a hexagonal wurtzite phase and free from pyrochlore phases.

Table 1
The structure parameters of ZnO-NPs calcinated at 650 °C and 750 °C.

Temperature °C	2θ	hkl	d_{hkl} (nm)	Structure	Lattice parameter (nm)	V $(nm)^3$	$Cos\varphi$
650	67.9	(112)	0.1379	Hexagonal	$a = 0.3222$	47.99	0.8480
	69.0	(201)	0.1360		$c/a = 1.6562$		
750	68.0	(112)	0.1378	Hexagonal	$a = 0.3224$	47.75	0.8479
	69.0	(201)	0.1390		$c/a = 1.6456$		

3.2. Particle size and strain

3.2.1. Scherrer method

XRD can be utilized to evaluate peak broadening with crystallite size and lattice strain due to dislocation [19]. The particle size of the ZnO-NPs was determined by the X-ray line broadening method using the Scherrer equation: $D = (k\lambda/\beta_D cos\theta)$, where D is the particle size in nanometers, λ is the wavelength of the radiation (1.54056 A° for CuK_α radiation), k is a constant equal to 0.94, β_D is the peak width at half-maximum intensity and θ is the peak position. The breadth of the Bragg peak is a combination of both instrument- and sample-dependent effects. To decouple these contributions, it is necessary to collect a diffraction pattern from the line broadening of a standard material such as silicon to determine the instrumental broadening. The instrument-corrected broadening [20] β_D corresponding to the diffraction peak of ZnO was estimated using the relation:

$$\beta_D^2 = \left[\left(\beta^2\right)_{measured} - \beta_{insturmental}^2\right] \Rightarrow \tag{4}$$

$$D = \frac{k\lambda}{\beta_D cos\theta} \Rightarrow cos\theta \frac{k\lambda}{D}\left(\frac{1}{\beta_D}\right) \tag{5}$$

Plots were drawn with $1/\beta_D$ on the x-axis and $cos\theta$ along the y-axis for the ZnO-NPs prepared at different temperatures such that the preferred orientation peaks of ZnO with the wurtzite hexagonal phase appeared between $2\theta = 20°$ and 100°. By fitting the data, the crystallite size D was extracted from the slope of the fit line; see Fig. 3.

3.2.2. Williamson–Hall methods

Strain-induced broadening arising from crystal imperfections and distortion are related by $\varepsilon \approx \beta_s/tan\theta$. A remarkable property of Eq. (5) is the dependency on the diffraction angle θ. The W–H method does not follow a $1/cos\theta$ dependency as in the Scherrer equation but instead varies with $tan\theta$. This fundamental difference allows for a separation of reflection broadening when both microstructural causes – small crystallite size and microstrain – occur together. The different approaches presented in the following assume that size and strain broadening are additive components of the total integral breadth of a Bragg peak [21]. The distinct θ dependencies of both effects laid the basis for the separation of size and strain broadening in the analysis of Williamson and Hall. Addition of the Scherrer equation and $\varepsilon \approx \beta_s/tan\theta$ results in following equations:

$$\beta_{hkl} = \beta_s + \beta_D \tag{6}$$

$$\beta_{hkl} = \left(\frac{k\lambda}{Dcos\theta}\right) + (4\varepsilon tan\theta) \tag{7}$$

Rearranging Eq. (7) gives:

$$\beta_{hkl} cos\theta = \left(\frac{k\lambda}{D}\right) + (4\varepsilon sin\theta) \tag{8}$$

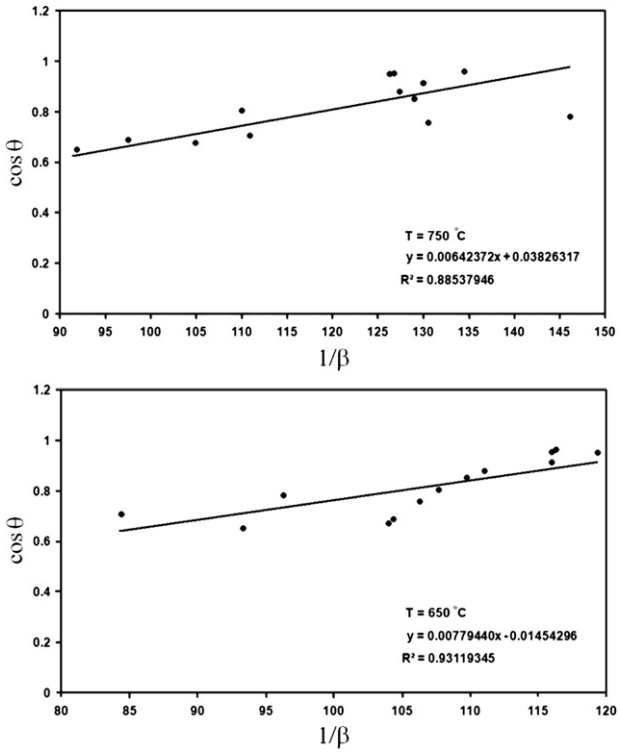

Fig. 3. Sherrer plot of ZnO-NPs calcinated at 650 °C and 750 °C. Fit to the data, the crystalline size D is extracted from the slope of the fit.

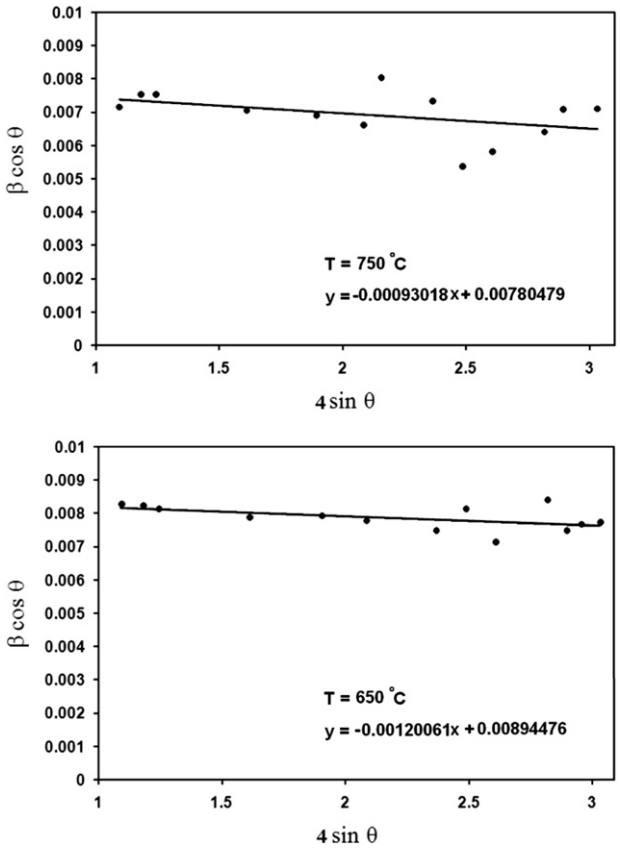

Fig. 4. The W–H analysis of ZnO-NPs calcinated at 650 °C and 750 °C assuming UDM. Fit to the data, the strain is extracted from the slope and the crystalline size is extracted from the y-intercept of the fit.

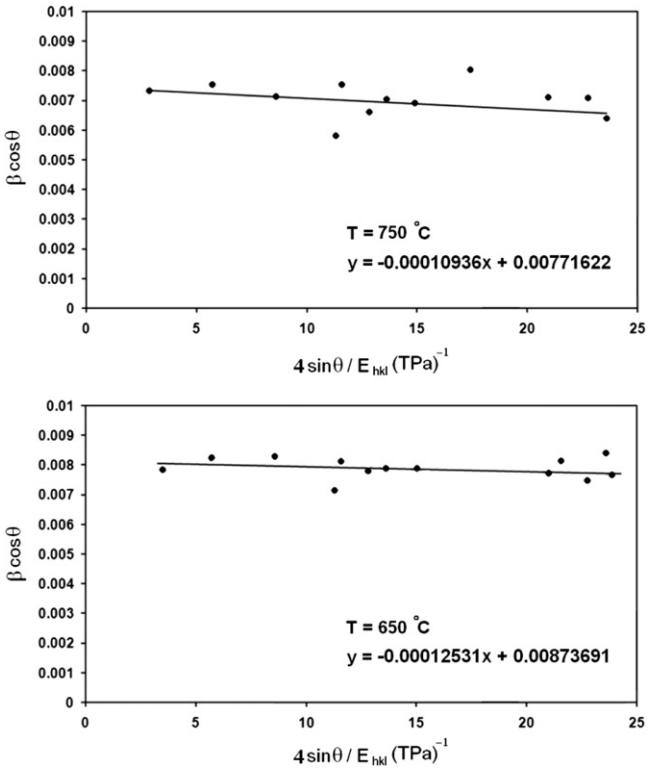

Fig. 5. The modified form of W–H analysis assuming USDM for ZnO-NPs calcinated at 650 °C and 750 °C. Fit to the data, the stress is extracted from the slope and the crystalline size is extracted from the *y*-intercept of the fit.

Eq. (8) represents the UDM, where the strain was assumed to be uniform in all crystallographic directions, thus considering the isotropic nature of the crystal, where all the material properties are independent of the direction along which they are measured. The term ($\beta\ cos\theta$) was plotted with respect to ($4\ sin\theta$) for the preferred orientation peaks of ZnO-NPs with the wurtzite hexagonal phase. Accordingly, the slope and *y*-intersect of the fitted line represent strain and particle size, respectively. The plots showed a negative strain for the ZnO-NPs. This strain may be due to the lattice shrinkage that was observed in the calculation of lattice parameters. The results of the UDM analysis for the ZnO-NPs are shown in Fig. 4.

In the Uniform Stress Deformation Model, USDM, a generalized Hooke's law refers to the strain, keeping only the linear proportionality between the stress and strain as given by $\sigma = Y\varepsilon$, where σ is the stress of the crystal and Y is the modulus of elasticity or Young's modulus. This equation is merely an approximation that is valid for a significantly small strain. Assuming a small strain to be present in the ZnO-NPs, Hooke's law can be used here. With a further increase in strain, the particles deviate from this linear proportionality. Applying the Hooke's law approximation to Eq. (8) yields:

$$\beta_{hkl}cos\theta = \left(\frac{k\lambda}{D}\right) + \left(\frac{4\sigma sin\theta}{Y_{hkl}}\right) \tag{9}$$

For a hexagonal crystal, Young's modulus is given by the following relation [14]:

$$Y_{hkl} = \frac{\left[h^2 + \frac{(h+2k)^2}{3} + \left(\frac{al}{c}\right)^2\right]^2}{s_{11}\left(h^2 + \frac{(h+2k)^2}{3}\right)^2 + s_{33}\left(\frac{al}{c}\right)^4 + (2s_{13} + s_{44})\left(h^2 + \frac{(h+2k)^2}{3}\right)\left(\frac{al}{c}\right)^2} \tag{10}$$

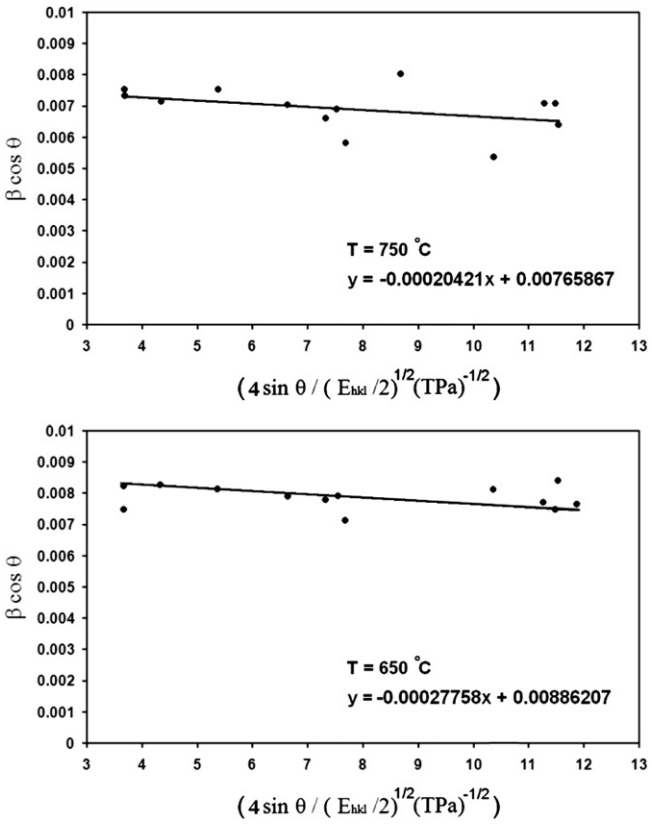

Fig. 6. The modified form of W–H analysis assuming UDEDM for ZnO-NPs calcinated at 650 °C and 750 °C. Fit to the data, the density of energy is extracted from the slope and the crystalline size is extracted from the *y*-intercept of the fit.

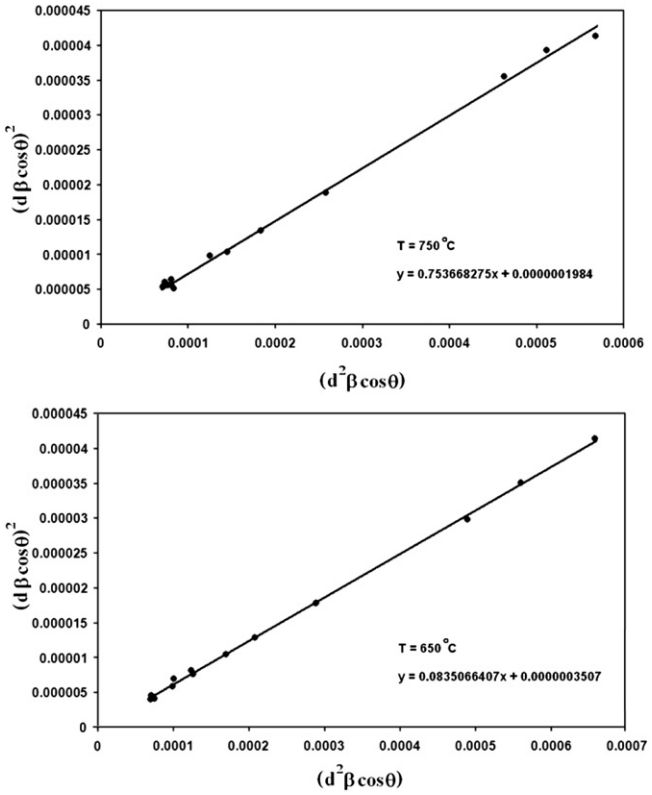

Fig. 7. The SSP plot of ZnO-NPs calcinated at 650 °C and 750 °C. The particle size is achieved from the slop of the liner fitted data and the root of *y*-intercept gives the strain.

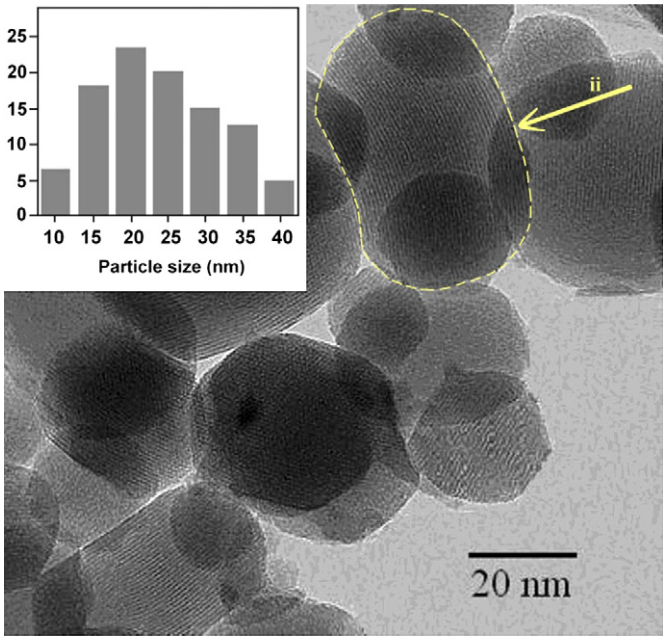

Fig. 8. TEM micrographs of ZnO-NPs calcinated at 750 °C. This figure shows a nonuniform strain for some of the ZnO-NPs (ii as an example). The size distribution and abundance of the ZnO-NPs was shown in inset.

where s_{11}, s_{13}, s_{33}, s_{44} are the elastic compliances of ZnO with values of 7.858×10^{-12}, -2.206×10^{-12}, 6.940×10^{-12}, 23.57×10^{-12} m^2 N^{-1}, respectively [22]. Young's modulus, *Y*, for hexagonal ZnO-NPs was calculated as ~130 GPa. Plots were drawn with $(4\ sin\ \theta)/Y_{hkl}$ on the *x*-axis and $\beta_{hkl}\ cos\theta$ on the *y*-axis for the ZnO-NPs calcined at different temperatures. The USDM plots for ZnO-NPs calcined at 650 °C and 750 °C are shown in Fig. 5. The stress calculated from the slope of the fitted line is slightly greater for the ZnO-NPs calcined at 650 °C than for those at 750 °C.

There is another model that can be used to determine the energy density of a crystal called the Uniform Deformation Energy Density Model, UDEDM. In Eq. (9), the crystals are assumed to have a homogeneous, isotropic nature. However, in many cases, the assumption of homogeneity and isotropy is not justified. Moreover, the constants of proportionality associated with the stress–strain relation are no longer independent when the strain energy density *u* is considered. For an elastic system that follows Hooke's law, the energy density *u* (energy per unit) can be calculated from $u = (\varepsilon^2 Y_{hkl})/2$. Then Eq. (9) can be rewritten according the energy and strain relation.

$$\beta_{hkl}cos\theta = \left(\frac{k\lambda}{D}\right) + \left(4sin\theta\left(\frac{2u}{Y_{hkl}}\right)^{1/2}\right) \tag{11}$$

Plots of $\beta_{hkl}\ cos\theta$ versus $4\ sin\theta(2u/Y_{hkl})^{1/2}$ were constructed and the data fitted to lines. The anisotropic energy density *u* was estimated from the slope of these lines, and the crystallite size *D* from the *y*-intercept; see Fig. 6. Previously, we had $\sigma = \varepsilon Y$ and $u = (\varepsilon^2 Y_{hkl})/2$, where the stress σ was calculated as $u = (\sigma^2/2Y_{hkl})$. The results of these plots show a slight change in energy density of the ZnO-NPs with increasing calcination temperature.

3.2.3. Size-strain plot method

The corresponding Williamson–Hall plot showed that line broadening was essentially isotropic. This indicates that the diffracting domains were isotropic and there was also a microstrain contribution. However, in cases of isotropic line broadening, a better evaluation of the size–strain parameters can be obtained by considering an average "size–strain plot" (SSP), which has the advantage that less weight is given to data from reflections at high angles, where the precision is usually lower. In this approximation, it is assumed that the "crystallite size" profile is described by a Lorentzian function and the "strain profile" by a Gaussian function [23]. Accordingly, we have:

$$(d_{hkl}\beta_{hkl}cos\theta)^2 = \frac{K}{D}\left(d_{hkl}^2\beta_{hkl}cos\theta\right) + \left(\frac{\varepsilon}{2}\right)^2 \tag{12}$$

Where *K* is a constant that depends on the shape of the particles; for spherical particles it is given as 3/4. In Fig. 7, similarly to the W–H methods, the term $(d_{hkl}\beta_{hkl}\ cos\theta)^2$ is plotted with respect to $(d_{hkl}^2\beta_{hkl}\ cos\theta)$ for the all orientation peaks of ZnO-NPs with the wurtzite hexagonal phase from $2\theta = 15°$ to $2\theta = 100°$. In this case, the particle size is determined from the slope of the linearly fitted data and the root of the *y*-intercept gives the strain.

3.2.4. TEM method

TEM micrographs are the best way to investigate nanoparticle size and shape. Fig. 8 displays a TEM image of the ZnO-NPs. It was observed that the morphology of the ZnO-NPs was spherical and with a smooth surface. The typical micrographs consisted of an assembly of ZnO-NPs with an average diameter of 20 ± 2 nm. A nonuniform strain was also observed that for some of the particles, as shown in Fig. 8. This is in close agreement with the results obtained from the powder XRD measurements.

The results obtained from the Scherrer method, UDM, USDM, UDEDM, SSP models and TEM are summarized in Table 2. The values of average crystallite size of the ZnO-NPs obtained from the different models are more or less similar, implying that the inclusion of strain in various forms has a very small effect on the average crystallite size of ZnO-NPs. However, the average crystallite size obtained from the Scherrer formula and the W–H analysis (see Table 2) shows a greater variation because of the difference in averaging the particle size distribution. By inspection of the plots, it appears that the result of the SSP model was more accurate than the UDM, USDM and UDEDM methods, as the data were fitted more accurately in this method, with all data points touching the fitting line.

Table 2
Geometric parameters of ZnO-NPs calcinated at 650 °C and 750 °C.

Sample	Scherrer method	Williamson–Hall method									Size–Strain Plot method				TEM
		UDM		USDM			UDEDM								
	D (nm)	*D* (nm)	ε no unit $\times 10^{-3}$	*D* (nm)	ε no unit $\times 10^{-3}$	σ (MPa)	*D* (nm)	ε no unit $\times 10^{-3}$	σ (MPa)	*u* (KJm^{-3})	*D* (nm)	ε no unit $\times 10^{-3}$	σ (MPa)	*u* (KJm^{-3})	*D* (nm)
650	18.58	16.19	1.2006	16.57	0.9867	125.31	16.34	1.1015	139.90	77.051	15.97	1.1843	150.41	89.681	–
750	22.54	18.55	0.9302	18.77	0.8611	109.36	18.91	0.8104	102.92	41.702	17.69	0.8908	113.13	50.393	~20

4. Conclusions

ZnO-NPs were synthesized by a sol–gel combustion process and characterized by powder XRD and TEM. The XRD indicated that the wurtzite structure ZnO-NPs were free from any pyrochlore phase at calcination temperatures of 650 °C and 750 °C. The line broadening of ZnO-NPs calcined at 650 °C and 750 °C was due to the small crystallite size and lattice strain. This broadening was analyzed by the Scherrer formula, modified forms of W–H analysis and the size–strain plot method. From the results, it was observed that the strain value decreased but the particle size increased as calcination temperature was increased. The TEM image of ZnO-NPs calcined at 750 °C revealed an average particle size of about 20 ± 2 nm and a nonuniform strain in the particles. The TEM results were in good agreement with the results of the W–H and the SSP methods.

Acknowledgements

This work was supported by university of Malaya through grants no: PS331\2009C and University Malaya HIRGA J-00000-73583.

References

[1] S. Hingorani, V. Pillai, P. Kumar, M.S. Muntai, D.O. Shah, Mater. Res. Bull. 28 (1993) 1303.
[2] S. Sakohara, M. Ishida, M.A. Anderson, J. Phys. Chem. B. 102 (1998) 10169.
[3] X. Zhao, S.C. Zhang, C. Li, B. Zheng, H. Gu, J. Mater. Synth. Process. 5 (1997) 227.
[4] A. Bandyopadhyay, S. Modak, S. Acharya, A.K. Deb, P.K. Chakrabarti, Solid State Sci. 12 (2010) 448.
[5] M.R. Vaezi, S.K. Sadrnezhaad, Mater. Des. 28 (2007) 515.
[6] A. Amiable, M.T. Buscaglia, V. Buscaglia, P. Bowen, J. Eur. Ceram. Soc. 30 (2010) 591.
[7] N. Riahi-Noori, R. Sarraf-Mamoory, P. Alizadeh, A. Mehdikhani, J. Ceram. Process. Res. 9 (2008) 246.
[8] T.S. Ko, S. Yang, H.C. Hsu, C.P. Chu, H.F. Lin, S.C. Liao, T.C. Lu, H.C. Kuo, W.F. Hsieh, S.C. Wang, Mater. Sci. Eng. B. 134 (2006) 54.
[9] S.B. Park, Y.C. Kang, J. Aerosol. Sci. 28 (1997) 473.
[10] W.S. Chiu, P.S. Khiew, D. Isa, M. Cloke, S. Radiman, R. Abd-Shukor, M.H. Abdullah, N.M. Huang, Chem. Eng. J. 142 (2008) 337.
[11] W. Bai, K. Yu, Q. Zhang, X. Zhu, D. Peng, Z. Zhu, N. Dai, Y. Sun, Physica E Low Dimens. Syst. Nanostruct. 40 (2008) 822.
[12] H. Bai, X. Liu, Mater. Lett. 64 (2010) 341.
[13] K. Ramakanth, Basic of Diffraction and Its Application. I.K. International Publishing House Pvt. Ltd, New Dehli, 2007.
[14] J. Zhang, Y. Zhang, K.W. Xu, V. Ji, Solid State Commun. 139 (2006) 87.
[15] N.S. Ramgir, Y.K. Hwang, I.S. Mulla, J.S. Chang, Solid State Sci. 8 (2006) 359.
[16] V.K. Pecharsky, P.Y. Zavalij, Fundamentals of Powder Diffraction and Structural Characterization of Materials. Springer, New York, 2003.
[17] C. Suranarayana, M.G. Norton, X-ray Diffraction: A Practical Approach New York (1998).
[18] B.D. Cullity, Elements of X-ray Diffraction. Addison-Wesley Publishing Company Inc., California, 1956.
[19] R. Yogamalar, R. Srinivasan, A. Vinu, K. Ariga, A.C. Bose, Solid State Commun. 149 (2009) 1919.
[20] K.D. Rogers, P. Daniels, Biomaterials 23 (2002) 2577.
[21] M. Birkholz, Thin Film Analysis by X-ray Scattering. Wiley-VCH Verlag GmbH and Co. KGaA, Weinheim, 2006.
[22] J.F. Nye, Physical Properties of Crystals: Their Representation by Tensors and Matrices. Oxford, New York, 1985.
[23] M.A. Tagliente, M. Massaro, Nucl. Instrum Methods Phys. Res. B. 266 (2008) 1055.
[24] A.K. Zak, M.E. Abrishami, W.H. Abd. Majid, R. Yousefi, S.M. Hosseini, Ceram. Inter. 37 (2011) 393.